Free Vibrations of a Taut Cable with Attached Damper. I: Linear Viscous Damper

By J.A. Main,[1] Student Member, ASCE, and N.P. Jones,[2] Member, ASCE

Abstract: Free vibrations of a taut cable with an attached linear viscous damper are investigated in detail using an analytical formulation of the complex eigenvalue problem. This problem is of considerable practical interest in the context of stay-cable vibration suppression in bridges. An expression for the eigenvalues is derived that is independent of the damper coefficient, giving the range of attainable modal damping ratios and corresponding oscillation frequencies in every mode for a given damper location without approximation. This formulation reveals the importance of damper-induced frequency shifts in characterizing the response of the system. New regimes of behavior are observed when these frequency shifts are large, as is the case in higher modes and for damper locations further from the end of the cable. For a damper located sufficiently near the antinode in a given mode, a regime of solutions is identified for which the damping approaches critical as the damper coefficient approaches a critical value. A regime is developed to indicate the type of behavior in each mode for any given damper location.

[1] Grad. Student, Dept. of Civil Engrg., Johns Hopkins Univ., 207 Latrobe Hall, 3400 N. Charles Street, Baltimore, MD, 21218. (410) 516-4136, FAX: (410) 516-7473, jmain@jhu.edu

[2] Prof. and Chair, Dept. of Civil Engrg., Johns Hopkins Univ., 207 Latrobe Hall, 3400 N. Charles Street, Baltimore, MD 21218. (410) 516-7874, FAX: (410) 516-7473, nick@jhu.edu

NOTE: This is the author's version of an article that was accepted for publication in Journal of Engineering Mechanics. A definitive version is available at http://dx.doi.org/doi:10.1061/(ASCE)0733-9399(2002)128:10(1072)

INTRODUCTION

The problem of large-amplitude stay vibrations on cable-stayed bridges is now quite well known, and vibration mitigation has become a significant concern to engineers in the design of new bridges and for retrofit of existing bridges (e.g., Poston 1998; Main and Jones 1999). Stay cables have very low levels of inherent mechanical damping, rendering them susceptible to multiple types of excitation (Yamaguchi and Fujino 1998). To suppress the problematic vibrations, viscous dampers are often attached to the stays near the anchorages. Although the mechanisms that induce the observed vibrations are still not fully understood, the effectiveness of attached dampers has been demonstrated; long-term measurements by the authors on three cable-stayed bridges indicate a significant reduction in vibration amplitudes after damper installation (Main and Jones 2001a). The potential for widespread application of dampers for cable vibration suppression necessitates a thorough understanding of the resulting dynamic system.

Carne (1981) and Kovacs (1982) were among the first to investigate the vibrations of a taut cable with an attached damper, both focusing on determination of first-mode damping ratios for damper locations near the end of the cable; Carne developed an approximate analytical solution, obtaining a transcendental equation for the complex eigenvalues and an accurate approximation for the first-mode damping ratio as a function of the damper coefficient and location, while Kovacs developed approximations for the maximum attainable damping ratio (in agreement with Carne) and the corresponding optimal damper coefficient (about 60% in excess of Carne's accurate result). Subsequent investigators formulated the free-vibration problem using Galerkin's method, with the sinusoidal mode shapes of an undamped cable as basis functions, and several hundred terms were required for adequate convergence in the solution, creating a computational burden (Pacheco et al. 1993). Several investigators have worked to develop modal damping estimation curves of general applicability (Yoneda and Maeda 1989; Pacheco et al. 1993), and Pacheco et al. (1993) introduced nondimensional parameters to develop a "universal estimation curve" of normalized modal damping ratio versus normalized damper coefficient, which is useful and applicable in many practical design situations. To consider the influence of cable sag and inclination on attainable damping ratios, Xu et al. (1997) developed an efficient and accurate transfer matrix formulation using complex eigenfunctions. Recently, Krenk (2000) developed an exact analytical solution of the free-vibration problem for a taut cable and obtained an asymptotic approximation for the damping ratios in the first few

modes for damper locations near the end of the cable; Krenk also developed an efficient iterative method for accurate determination of modal damping ratios outside the range of applicability of the asymptotic approximation.

Previous investigations have focused on vibrations in the first few modes for damper locations near the end of the cable, and while practical constraints usually limit the damper attachment location, it is important to understand both the range of applicability of previous observations and the behavior that may be expected outside of this range. Damper performance in the higher modes is of particular interest, as full-scale measurements by the writers (Main and Jones 2000) indicate that vibrations of moderate amplitude can occur over a wide range of cable modes. In this paper an analytical formulation of the free-vibration problem is used to investigate the dynamics of the cable-damper system in higher modes and without restriction on the damper location. The basic problem formulation in this paper follows quite closely the approach recently used by Krenk (2000), although it was developed independently as an extension of the transfer matrix technique developed by Iwan (Sergev and Iwan, 1981; Iwan and Jones 1984) to calculate the natural frequencies and mode shapes of a taut cable with attached springs and masses. A similar approach was used by Rayleigh (1877) to consider the vibrations of a taut string with an attached mass. Using this formulation, the important role of damper-induced frequency shifts in characterizing the system is observed and emphasized. Consideration of the nature of these frequency shifts affords additional insight into the dynamics of the system, and when the shifts are large, complicated new regimes of behavior are observed.

The influences of sag and bending stiffness are neglected in the present paper, because the linear taut-string approximation is considered applicable to many real stay cables, and the simplifications introduced by these approximations allow for a more efficient formulation of the problem and a more detailed investigation of the dynamics of the system. It has been shown that moderate amounts of sag can significantly reduce the first-mode damping ratio, while the damping ratios in the higher modes are virtually unaffected (Pacheco et al. 1993; Xu et al. 1999). However, using a database of stay cable properties from real bridges, Tabatabai and Mehrabi (2000) found that for most actual stays, the influence of sag is insignificant, even in the first mode. Tabatabai and Mehrabi (2000) did find that the influence of bending stiffness could be significant for many stays, especially for damper locations quite near the end of

the cable, and the present writers have carried out a detailed study of the influence of bending stiffness, to be presented in a subsequent publication.

PROBLEM FORMULATION

The problem under consideration is depicted in Fig. 1. The damper is attached to the cable at an intermediate point, dividing the cable into two segments, where $\ell_2 > \ell_1$. Assuming that the tension in the cable is large compared to its weight, bending stiffness and internal damping are negligible, and deflections are small, the following partial differential equation is satisfied over each segment of cable:

$$m\frac{\partial^2 y_k(x_k,t)}{\partial t^2} = T\frac{\partial^2 y_k(x_k,t)}{\partial {x_k}^2} \tag{1}$$

where $y_k(x_k,t)$ is the transverse deflection and x_k is the coordinate along the cable chord axis in the k^{th} segment; m is the mass per unit length, and T is the tension in the cable. This equation is valid everywhere except at the damper attachment point; at this location continuity of displacement and equilibrium of forces must be satisfied. As in Pacheco et al. (1993), a nondimensional time $\tau = \omega_{o1}t$ is introduced, where $\omega_{o1} = (\pi/L)\sqrt{T/m}$. To solve (1) subject to the boundary, continuity, and equilibrium conditions, distinct solutions over the two cable segments are assumed of the form:

$$y_k(x_k,\tau) = Y_k(x_k)e^{\lambda\tau} \tag{2}$$

where λ is a dimensionless eigenvalue that is complex in general[1]. Substituting (2) into (1) yields the following ordinary differential equation:

$$\frac{d^2Y_k(x_k)}{dx_k^2} = \left(\frac{\pi\lambda}{L}\right)^2 Y_k(x_k) \tag{3}$$

Because λ is complex, the solutions to (3), which are the mode shapes of the system, are also complex. Continuity of displacement at the damper and the boundary conditions of zero displacement at the cable ends can be enforced by expressing the solution as

[1] The assumed solution may be alternatively expressed as $y_k(x_k,\tau) = Y_k(x_k)e^{j\omega\tau}$, where $j = \sqrt{-1}$ and ω is complex; this alternative formulation leads to trigonometric rather than hyperbolic expressions for the eigenfunctions. Although the two forms are equivalent, when the damping is small, ω is "mostly" real, and this alternative form leads to more direct expressions for the eigenfunctions. In cases of large damping, to be discussed herein, λ is "mostly" real, and the form of solution in (2) is more direct.

$$Y_k(x_k) = \gamma \frac{\sinh(\pi\lambda\, x_k / L)}{\sinh(\pi\lambda\, \ell_k / L)} \tag{4}$$

where γ is the amplitude at the damper. The equilibrium equation at the damper can be written as

$$T\left[-\frac{\partial y_2}{\partial x_2}\Big|_{x_2=\ell_2} - \frac{\partial y_1}{\partial x_1}\Big|_{x_1=\ell_1} \right] = c\frac{\partial y_1}{\partial t}\Big|_{x_1=\ell_1} \tag{5}$$

where c is the damper coefficient. Differentiating the assumed solution [(2) and (4)] and substituting into (5) yields:

$$\coth(\pi\lambda\, \ell_1 / L) + \coth(\pi\lambda\, \ell_2 / L) + \frac{c}{\sqrt{Tm}} = 0 \tag{6}$$

Eq. (6) is equivalent to the "frequency equation" presented by Krenk (2000). Its roots are the eigenvalues of the system, each corresponding to a distinct mode of vibration. For specific values of $c/\sqrt{Tm}$ and ℓ_1/L, (6) can be directly solved numerically to obtain the damping ratios in as many modes as desired to an arbitrary degree of accuracy. Each eigenvalue can be written explicitly in terms of real and imaginary parts as follows

$$\lambda_i = \frac{\omega_i}{\omega_{o1}}\left(-\zeta_i + j\sqrt{1-\zeta_i^2} \right) \tag{7}$$

in which ζ_i is the damping ratio and ω_i is the modulus of the dimensional eigenvalue, which has been referred to as the pseudoundamped natural frequency (Pacheco et al. 1993). For convenience in subsequent manipulations, new symbols are introduced to denote the real and imaginary parts of the i^{th} eigenvalue:

$$\sigma_i = \mathrm{Re}(\lambda_i)\,; \;\; \varphi_i = \mathrm{Im}(\lambda_i) \tag{8a,b}$$

It is noted that φ_i is the nondimensional frequency of damped oscillation. The damping ratio ζ_i can be computed from σ_i and φ_i:

$$\zeta_i = \left(\frac{\varphi_i^{\,2}}{\sigma_i^{\,2}} + 1 \right)^{-\frac{1}{2}} \tag{9}$$

Further insight into the solution characteristics can be obtained by expanding (6) explicitly into real and imaginary parts. Taking the imaginary part of (6) and expanding using the notation of (8a,b) yields the following equation, after some simplification:

$$\sin(2\pi\varphi\,\ell_1/L)\cosh(2\pi\sigma\,\ell_2/L)+\sin(2\pi\varphi\,\ell_2/L)\cosh(2\pi\sigma\,\ell_1/L)=\sin(2\pi\varphi) \tag{10}$$

This equation is independent of $c/\sqrt{Tm}$, and its solution branches give permissible values of λ for a given ℓ_1/L, thus revealing the attainable values of modal damping with their corresponding oscillation frequencies. Because it corresponds to enforcing equality of phase in (5), (10) will be referred to herein as the "phase equation". While solution branches to (10) are symmetric about σ=0, only negative values of σ are considered, as positive values of σ are associated with negative values of $c/\sqrt{Tm}$, which are not of practical interest. Taking the real part of (6) yields the following equation, after some simplification:

$$\frac{\sinh(2\pi\sigma\,\ell_1/L)}{\cosh(2\pi\sigma\,\ell_1/L)-\cos(2\pi\varphi\,\ell_1/L)}+\frac{\sinh(2\pi\sigma\,\ell_2/L)}{\cosh(2\pi\sigma\,\ell_2/L)-\cos(2\pi\varphi\,\ell_2/L)}+\frac{c}{\sqrt{Tm}}=0 \tag{11}$$

For a specific value of λ with real and imaginary parts σ and φ that satisfy (10), the corresponding value of $c/\sqrt{Tm}$ can be readily computed from (11). The expression (4) for the complex mode shapes can be expanded explicitly in terms of the real and imaginary parts using the notation of (8a,b), yielding the following expression

$$Y_k(x_k)=A_k\left[\sinh(\pi\sigma\,x_k/L)\cos(\pi\varphi\,x_k/L)+j\cosh(\pi\sigma\,x_k/L)\sin(\pi\varphi\,x_k/L)\right] \tag{12}$$

in which the complex coefficients are given by $A_k=\gamma/\sinh(\pi\lambda\,\ell_k/L)$. This expression will be useful in considering the character of the mode shapes in the following sections, in which three special types of solutions will be considered: a non-oscillatory decaying solution (φ=0), non-decaying oscillatory solutions (σ=0), and oscillatory solutions approaching critical damping ($\sigma\rightarrow-\infty$ and $\zeta\rightarrow1$).

THE SPECIAL CASE OF NON-OSCILLATORY DECAY

Solutions to (6) can exist for which λ is purely real, corresponding to non-oscillatory, exponentially decaying solutions in time; in this case φ=0, the phase equation (10) is trivially satisfied, and (11) reduces to:

$$\frac{\sinh(-2\pi\sigma\,\ell_1/L)}{\cosh(-2\pi\sigma\,\ell_1/L)-1}+\frac{\sinh(-2\pi\sigma\,\ell_2/L)}{\cosh(-2\pi\sigma\,\ell_2/L)-1}=\frac{c}{\sqrt{Tm}} \tag{13}$$

in which it is emphasized that positive values of $c/\sqrt{Tm}$ are of practical interest, leading to negative values of σ. Eq. (13) reveals that purely real solutions exist only when $c/\sqrt{Tm}$ exceeds a critical value;

when $\sigma \rightarrow -\infty$, the two terms on the left-hand side of (13) each approach unity, so that the critical value of c associated with this limit is given by:

$$c_{crit} = 2\sqrt{Tm} \tag{14}$$

For $c<c_{crit}$ no solutions to (13) exist, as it can be shown that the left-hand side of (13) is always >2; for $c>c_{crit}$ the magnitude of σ decreases monotonically with increasing c. In the limit as $\sigma \rightarrow 0$, it can be shown that $c/\sqrt{Tm} \rightarrow \infty$. This case of non-oscillatory decay may be compared to the case of supercritical damping for a single-degree-of-freedom (SDOF) oscillator[1], for which the solution decays exponentially without oscillation, and the rate of decay decreases with increasing c. With $\varphi=0$ in this case, the expression for the the mode shapes (12) reduces to a hyperbolic sinusoid with a purely real argument:

$$Y_k(x_k) = A_k \sinh\left(\pi\sigma x_k / L\right) \tag{15}$$

Fig. 2 illustrates the mode shape corresponding to a purely real eigenvalue, plotted for several different values of $c/\sqrt{Tm}$, with an arrow indicating the trend with increasing c. As $c \rightarrow \infty$ and $\sigma \rightarrow 0$ according to (13), the linear term in the series expansion of $\sinh(\pi\sigma x_k / L)$ becomes dominant, and the mode shape tends to the static deflected shape of the cable under a concentrated load.

LIMITING CASES OF NON-DECAYING OSCILLATION

Solutions to (6) can exist for which λ is purely imaginary ($\sigma=0$), corresponding to non-decaying oscillation or zero damping. It can be shown that when $\sigma=0$, the phase equation (10) reduces to

$$\sin(\pi\varphi\,\ell_1/L)\sin(\pi\varphi\,\ell_2/L)\sin(\pi\varphi) = 0 \tag{16}$$

which indicates that there are three sets of frequencies associated with $\zeta=0$, corresponding to the zeros of each of the sinusoids in (16). One of these sets of frequencies is associated with the limit of $c \rightarrow 0$ and the other two sets of frequencies are associated with the limit of $c \rightarrow \infty$ (i.e., a perfectly rigid damper.) Many investigators have made reference to these limiting cases in giving a physical explanation for the existence of an optimum damper coefficient for a specific mode: in both of these limits, physical intuition suggests

[1] It is noted that the critical value of the damper coefficient for an SDOF oscillator has a remarkably similar form: $c_{crit} = 2\sqrt{km}$, where m is the mass and k is the spring constant.

that the damping ratios must be zero. These limiting cases can be observed more clearly by rearranging the eigenvalue equation (6) into the following form:

$$\sinh(\pi\lambda) + \frac{c}{\sqrt{Tm}}\sinh(\pi\lambda\,\ell_1/L)\sinh(\pi\lambda\,\ell_2/L) = 0 \tag{17}$$

In the first limiting case, when $c \rightarrow 0$, (17) reduces to $\sinh(\pi\lambda) = 0$, which can only be satisfied if λ is an integer multiple of $j = \sqrt{-1}$. Consequently, λ must be purely imaginary and φ must take on integer values:

$$\varphi_{oi} = i \tag{18}$$

These frequencies simply correspond to vibrations in the undamped natural modes of the cable. In the second limiting case, when $c \rightarrow \infty$, (17) becomes $\sinh(\pi\lambda\,\ell_1/L)\sinh(\pi\lambda\,\ell_2/L) = 0$, which yields two sets of roots, both of which are purely imaginary. One set of roots, corresponding to the zeros of $\sinh(\pi\lambda\,\ell_2/L)$, yields the following frequencies:

$$\varphi_{ci} = i(L/\ell_2) \tag{19}$$

These frequencies correspond to vibrations of the longer cable segment of length ℓ_2, with zero displacement at the damper (the subscript c indicates a "clamped" frequency). The second set of roots, corresponding to the zeros of $\sinh(\pi\lambda\,\ell_1/L)$, yields the following frequencies:

$$\varphi_{ci}^{(1)} = i(L/\ell_1) \tag{20}$$

These frequencies correspond to vibrations of the shorter cable segment of length ℓ_1 (the superscript indicates vibrations of the cable segment with index k=1), also with zero displacement at the damper. As the three sets of frequencies (18)-(20) represent all the solutions to (16), there no other frequencies associated with ζ=0. When σ=0, the expression for the mode shapes (12) reduces to:

$$Y_k(x_k) = A_k\, j \sin\left(\pi\varphi\, x_k/L\right) \tag{25}$$

which indicates that when the ζ=0, the mode shapes over each cable segment are sinusoids with purely real arguments. Fig. 3 depicts mode shapes associated with these three special cases of non-decaying oscillation; the mode shape associated with φ_{o1} is depicted in Fig. 3(a), and the mode shapes associated with φ_{c1} and $\varphi_{c1}^{(1)}$ are depicted in Figs. 3(b) and 3(c), respectively.

OSCILLATORY SOLUTIONS APPROACHING CRITICAL DAMPING

Complex-valued solutions to (6) can exist for which $\sigma \rightarrow -\infty$ as the nondimensional frequency φ tends to a constant value. When $\sigma \rightarrow -\infty$ with φ bounded, it is evident from (9) that $\zeta \rightarrow 1$, so that while the real part of the eigenvalue increases without limit, the damping ratio itself approaches a finite value ($\zeta=1$), corresponding to critical damping. The frequencies associated with these limiting cases of critical damping can be determined from the phase equation (14) by taking the limit as $\sigma \rightarrow -\infty$, which yields the equation $\sin(2\pi\varphi \ell_1 / L) = 0$. The frequencies that satisfy this equation can be divided into two distinct categories:

$$\varphi_{crit,i} = \left(i - 1/2\right)\left(L/\ell_1\right); \quad \varphi^{(1)}_{crit,i} = i\left(L/\ell_1\right) \tag{22a,b}$$

It is noted that the frequencies $\varphi_{crit,i}^{(1)}$ coincide with the clamped frequencies of the shorter cable segment in (20). It can be readily shown using (11) that as $\sigma \rightarrow -\infty$, $c/\sqrt{Tm} \rightarrow 2$, or $c \rightarrow c_{crit}$, regardless of the value of φ. As $\sigma \rightarrow -\infty$, the expression for the mode shapes (12) tends to

$$Y_k(x_k) \cong A_k \sinh\left(\pi\sigma x_k / L\right)\exp\left(j\pi\varphi x_k / L\right) \tag{23}$$

Eq. (23) indicates that as $\sigma \rightarrow -\infty$, the magnitude of the mode shape over each cable segment takes the same hyperbolic form as (15) for the case of non-oscillatory decay.

DAMPER PERFORMANCE FOR SMALL FREQUENCY SHIFTS

By focusing their attention on vibrations in the first few modes for small values of ℓ_1/L, previous investigators restricted their attention to cases in which the damper-induced frequency shifts are small. Consideration of the characteristics of solution branches to the phase equation (10) in these cases provides additional insight into the dynamics of the cable-damper system. Fig. 4 shows the first five branches of solutions to (10) for $\ell_1/L=0.05$ plotted in the φ-ζ plane; a distinct solution branch is associated with each mode. The frequencies associated with the special cases of non-decaying oscillation discussed above are plotted along the horizontal axis; the undamped frequencies, φ_{oi}, are indicated by circles and the clamped frequencies, φ_{ci}, are indicated by crosses. Each solution branch originates at φ_{oi} with $\zeta=0$, terminates at φ_{ci} with $\zeta=0$, and takes on nonzero values of ζ for intermediate frequencies. The difference between these two limiting frequencies is given by

$$\Delta\varphi_i = \varphi_{ci} - \varphi_{oi} = i\left(\ell_1 / \ell_2\right) \tag{24}$$

The similar form of the solution branches for each mode suggests that it may be useful to define a new parameter as a measure of the damper-induced frequency shift

$$\Theta_{ci} = \frac{\varphi_i - \varphi_{oi}}{\Delta\varphi_i}; \quad 0 \le \Theta_{ci} < 1 \tag{25}$$

The parameter, which will be referred to as the "clamping ratio" in the i^{th} mode, is zero when c=0, as depicted in Fig. 3(a), and it approaches unity when $c \rightarrow \infty$, as depicted in Fig. 3(b). The frequency of oscillation in mode i can then be expressed as

$$\varphi_i = i + \Theta_{ci}\Delta\varphi_i \tag{26}$$

When the frequency difference, $\Delta\varphi_i$, is small, σ_i is also small, and in this limit an approximate solution to (10) can be developed by substituting the expression for φ_i in (26) into (10) and expanding each term as a Taylor series. Solving the resulting approximate equation for σ_i and taking the limit of small $\Delta\varphi_i$ (which also implies small ℓ_1/L) yields the following expression:

$$\sigma_i \cong -i(\ell_1 / L)\sqrt{\Theta_{ci}(1-\Theta_{ci})} \tag{27}$$

Noting that $\zeta_i \approx -\sigma_i/i$, (27) yields the following asymptotic relation between the ζ_i and Θ_{ci}:

$$\frac{\zeta_i}{(\ell_1/L)} \cong \sqrt{\Theta_{ci}(1-\Theta_{ci})} \tag{28}$$

This relation is independent of mode number, indicating a maximum attainable damping ratio of $\zeta_i=(1/2)(\ell_1/L)$ in each mode, corresponding to an optimal clamping ratio of $\Theta_{ci}=1/2$. Fig. 5(a) shows a plot of the asymptotic solution (28), along with numerically computed curves of $\zeta_i/(\ell_1/L)$ versus Θ_{ci} in the first five modes for ℓ_1/L=0.02, generated by numerical solution of (10). A distinct curve is plotted for each mode, and for this damper location, the numerically generated curves corresponding to each of the five modes are indeed very nearly identical, agreeing quite well with (28). An approximate relation between the clamping ratio and $c/\sqrt{Tm}$ can be established by substituting the expressions for φ_i (26) and σ_i (27) into equation (11) and using similar asymptotic approximations, yielding the following relation:

$$\kappa \cong \frac{1}{\pi^2}\sqrt{\frac{\Theta_{ci}}{1-\Theta_{ci}}} \tag{29}$$

where κ is a nondimensional parameter grouping defined as

$$\kappa \equiv \frac{c}{mL\omega_{o1}} i \frac{\ell_1}{L} \tag{30}$$

It is noted that $c/\sqrt{Tm} = \pi c/(mL\omega_{o1})$, and the alternative normalization $c/(mL\omega_{o1})$ is used in (30) to facilitate comparison with previous investigations; κ is equivalent to the nondimensional parameter grouping plotted on the abscissa in the universal curve of Pacheco et al. (1993). Fig. 5(b) shows a plot of (29) along with numerically computed curves of κ versus Θ_{ci} in the first five modes for ℓ_1/L=0.02, generated from (11) after numerical solution of (10). Again, the numerically computed curves corresponding to each of the five modes are nearly identical, agreeing well with the approximation of (29). The clamping ratio increases monotonically with κ, from $\Theta_{ci} = 0$ when $\kappa = 0$ to approach $\Theta_{ci} = 1$ as $\kappa \rightarrow \infty$. Substituting the optimal clamping ratio of Θ_{ci}=1/2 into (29) reveals that the optimal value of modal damping is achieved when $\kappa = \pi^{-2} \approx 0.101$, as determined by Krenk (2000). Eq. (29) can be inverted and solved for Θ_{ci}:

$$\Theta_{ci} \cong \frac{(\pi^2\kappa)^2}{(\pi^2\kappa)^2 + 1} \tag{31}$$

Substituting this expression into (28) yields the following approximate relation:

$$\frac{\zeta_i}{(\ell_1/L)} \cong \frac{\pi^2\kappa}{(\pi^2\kappa)^2 + 1} \tag{32}$$

This expression was recently derived by Krenk (2000); it is an analytical expression for the "universal curve" of Pacheco et al. (1993) and is a generalization of the first-mode approximation obtained by Carne (1981). Fig. 5(c) shows a plot of (32) along with curves of $\zeta_i/(\ell_1/L)$ versus κ for the first five modes for ℓ_1/L=0.02 generated numerically from (10) and (11). It is evident that again the curves collapse very nearly onto a single curve in good agreement with the approximation of (32).

It is important to note that the optimal damping ratio can only be achieved in one mode for a linear damper. Noting that κ is proportional to mode number, it is evident from Fig. 5(b) that Θ_{ci} increases monotonically with mode number, so that if the damper is designed optimally for a particular mode, it will be effectively more rigid in the higher modes and more compliant in the lower modes, resulting in suboptimal damping ratios in other modes. As discussed in the companion paper (Main and Jones 2001b),

recent investigations by the writers indicate that nonlinear dampers may potentially overcome this limitation in performance, allowing the optimal damping ratio to be achieved in more than one mode; however, in the case of a nonlinear damper, the damping performance is amplitude-dependent, and optimal performance can only be achieved in the neighborhood of a particular oscillation amplitude.

DAMPER PERFORMANCE FOR LARGE FREQUENCY SHIFTS

When the frequency difference $\Delta\varphi_i$ in a given mode becomes large, as is the case in higher modes and for larger values of ℓ_1/L, the approximate relations (28), (29), and (32) become less accurate. Fig. 6 shows the same plot as in Fig. 5(c), but for a damper located further from the end of the cable, at ℓ_1/L=0.05, and a distinct curve has been plotted for each of the first eight modes, with an arrow indicating the trend with increasing mode number. It is evident that the curves no longer collapse together. The solution curves for the first few modes agree quite well with the curves in Fig. 5(c); however, as the mode number increases, yielding larger values of $\Delta\varphi_i$, departures become significant, and the optimal damping value $\zeta_{i,opt}/(\ell_1/L)$ and the corresponding abscissa value κ_{opt} both increase noticeably with mode number. Numerical investigation in the first five modes over a range of ℓ_1/L revealed that $\zeta_{i,opt}/(\ell_1/L)$ increases monotonically with $\Delta\varphi_i$ in a given mode, to take on a value of 1.2 - 1.3 as $\Delta\varphi_i \rightarrow 0.5$, and κ_{opt} also increases monotonically with $\Delta\varphi_i$, taking on a value of about 0.18 as $\Delta\varphi_i \rightarrow 0.5$. When $\Delta\varphi_i$ reaches 0.5 in a given mode, new regimes of behavior are observed which are discussed in the following sections.

Special Cases of Vertical Solution Branches

In investigating and categorizing the complicated characteristics of solution branches to the phase equation (10) for large frequency shifts, it useful to begin by considering some special cases of vertical solution branches, which serve as boundaries between different regimes of behavior. These branches extend from σ=0 to σ=–∞ [from ζ=0 to ζ=1 according to (13)] at a constant frequency φ. Inspection of (10) reveals that if the following conditions are satisfied:

$$\sin(2\pi\varphi\,\ell_1/L) = 0\,;\ \sin(2\pi\varphi\,\ell_2/L) = 0\,;\ \sin(2\pi\varphi) = 0 \qquad (33a,b,c)$$

then (10) is trivially satisfied for all values of σ, yielding a vertical solution branch. The values of φ that satisfy (33*a*) are the two sets of critically damped frequencies previously introduced in (22*a*,*b*). The condition (33*c*) is satisfied if φ can be expressed as i or as i+1/2, where i is an integer. It is noted that the

additional requirement (33b) follows directly from (33*a*) and (33*c*), and consequently, (33*a,b,c*) are all satisfied in four distinct cases, corresponding to four types of vertical solution branches. To aid in interpreting these special cases, Fig. 7 presents a plot of the different sets of nondimensional frequencies, φ_{oi} (18), φ_{ci} (19), $\varphi_{ci}^{(1)}$ (20) – which is equal to $\varphi_{crit,i}^{(1)}$ (22*b*), and $\varphi_{crit,i}$ (22*a*), against ℓ_1/L. The combinations of ℓ_1/L and φ corresponding to the four distinct types of vertical solution branches are indicated with different symbols. These four types are discussed in the following paragraphs, and the contexts in which they arise are discussed in subsequent sections. Along a vertical solution branch, (11) can be expressed as

$$\frac{\sinh(2\pi\sigma\,\ell_1/L)}{\cosh(2\pi\sigma\,\ell_1/L)+a}+\frac{\sinh(2\pi\sigma\,\ell_2/L)}{\cosh(2\pi\sigma\,\ell_2/L)+b}+\frac{c}{\sqrt{Tm}}=0 \tag{34}$$

where $a=-\cos(2\pi\varphi\,\ell_1/L)$ and $b=-\cos(2\pi\varphi\,\ell_2/L)$, and because φ is constant along each branch, *a* and *b* are also constant.

Type 1: $\varphi_{crit,n}=i$. In these cases, indicated with hollow circles in Fig. 7, the n^{th} critically damped frequency $\varphi_{crit,n}$ (22a), where *n* is an integer, coincides with an undamped frequency, $\varphi_{oi}=i$. Equating these expressions and solving for ℓ_1/L yields ℓ_1/L=(*n*-1/2)/*i*, where $n\le(i+1)/2$, which corresponds to a damper located at the n^{th} antinode of mode *i*. In this case, *a*=1 and *b*=1 in (34), from which it can be shown that for this case, $c/\sqrt{Tm}\rightarrow 2$ monotonically from zero as $\sigma\rightarrow-\infty$ from zero.

Type 2: $\varphi_{crit,n}=i+1/2$. In these cases, indicated with solid squares in Fig. 7, the n^{th} critically damped frequency, $\varphi_{crit,n}$ (22a), equals *i*+1/2. Equating these expressions and solving for ℓ_1/L yields ℓ_1/L=(*n*-1/2)/(*i*+1/2), where $n\le(i+1)/2$. It is also noted that in these cases $\varphi_{crit,n}$ coincides with a clamped frequency φ_{cp} (19), where *p* is also an integer. Using these expressions, the intersection frequency can be expressed in terms of *n* and *p* as (*i*+1/2)=*n*+*p*-1/2, and the corresponding damper location can be expressed as ℓ_1/L = (*n*-1/2)/(*n*+*p*-1/2), where $n\le p$. In this case, *a*=1 and *b*=–1 in (34), and using the resulting expression it can be shown that $c/\sqrt{Tm}$ takes on a minimum value of $(1+\ell_1/\ell_2)\sinh(-2\pi\sigma_o\,\ell_1/L)/[\cosh(-2\pi\sigma_o\,\ell_1/L)+1]$, which is less than 2, at a value σ_o which satisfies the equation $(\ell_1/L)\cosh(-2\pi\sigma\,\ell_2/L)-(\ell_2/L)\cosh(-2\pi\sigma\,\ell_1/L)=1$. As σ decreases from σ_o to approach zero, $c/\sqrt{Tm}$ increases monotonically to approach infinity, and as σ increases from

σ_o to approach infinity, $c/\sqrt{Tm}$ increases monotonically to approach 2. It will be observed subsequently that this type of vertical solution branch actually corresponds to two solution branches that intersect at the intermediate value $\sigma=\sigma_o$ and diverge; along one branch $\sigma\rightarrow-\infty$ as $c/\sqrt{Tm}\rightarrow 2$, and along the other branch $\sigma\rightarrow 0$ as $c/\sqrt{Tm}\rightarrow\infty$.

Type 3: $\varphi_{crit,n}^{(1)} = i$. In these cases, indicated with solid circles in Fig. 7, the n^{th} critically damped frequency associated with the shorter cable segment, $\varphi_{crit,n}^{(1)}$ (22b), coincides with an undamped frequency, $\varphi_{oi}=i$. Equating these expressions and solving for ℓ_1/L yields $\ell_1/\mathrm{L}=n/i$, where $n\leq i/2$, which corresponds to a damper located at the n^{th} node of mode i. In this case, $a=-1$ and $b=-1$ in (34), and the resulting expression is the same as (13) for the case of a purely real eigenvalue, for which it was observed that $c/\sqrt{Tm}$ increases monotonically from 2 to approach infinity as $\sigma\rightarrow 0$ from $-\infty$.

Type 4: $\varphi_{crit,n}^{(1)} = i+1/2$. In these cases, indicated with hollow squares in Fig. 7, the n^{th} critically damped frequency associated with the smaller cable segment, $\varphi_{crit,n}^{(1)}$ (22b), equals $i+1/2$. Equating these expressions and solving for ℓ_1/L yields $\ell_1/L=n/(i+1/2)$, where $n\leq i/2$. In this case, $a=-1$ and $b=1$ in (34), and it can be shown that $c/\sqrt{Tm}$ increases monotonically from 2 to approach infinity as $\sigma\rightarrow 0$ from $-\infty$.

Behavior in a Single Mode

To further explore the dynamics of the cable-damper system, is it helpful to consider the evolution of a single solution branch of the phase equation (10) as the damper is moved from the end of the cable past the first antinode to the first node of the corresponding undamped mode; over this range, three distinct regimes of behavior are observed for a given mode. The evolution of the solution branch associated with mode 2 will be considered, and Fig. 8 shows a surface plot of ζ versus φ and ℓ_1/L for mode 2; the surface was generated by incrementing ℓ_1/L from 0 to 0.5 and repeatedly solving (10). Fig. 9 is a companion to Fig. 8 with a separate plot for each of the three regimes; each curve in Fig. 9 is a slice through the surface of Fig. 8 at a specific value of ℓ_1/L.

Regime 1: Characteristics of regime 1 are exhibited in a given mode i when $0\leq\ell_1/\mathrm{L}<1/(2i+1)$; the upper limit of ℓ_1/L is associated with a vertical solution branch of type 2 at $\varphi=i+1/2$. Fig. 9(a) shows curves of ζ versus φ within regime 1 for mode 2, and the characteristics of these solution branches are similar to those previously observed. Each curve originates at the undamped frequency φ_{oi} (18) with $\zeta=0$ (indicated

by a circle), terminates at the clamped frequency φ_{ci} (19) with ζ=0 (indicated by a cross), and attains a maximum value of ζ at an intermediate frequency. The width of the base of the curve is $\Delta\varphi_i$, and as ℓ_1/L is increased within this regime, $\Delta\varphi_i$ increases and larger values of ζ are attained. As $\ell_1/L \rightarrow 1/(2i+1)$ and $\Delta\varphi_i \rightarrow 1/2$, the shape of the curve becomes increasingly skewed to the right.

Intermediate Case: When $\ell_1/L=1/(2i+1)$, $\Delta\varphi_i=1/2$, and the clamped frequency $\varphi_{ci}=i+1/2$. For this value of ℓ_1/L, the first critically damped frequency $\varphi_{crit,1}$ (22a) also equals i+1/2, and a vertical solution branch of type 2 occurs at $\varphi=i+1/2$, with the solution branches for mode i and mode i + 1 intersecting at this intermediate frequency. This situation is depicted in Fig. 10 for ℓ_1/L=0.2; in this case the solution branches for modes 2 and 3 intersect at φ=2.5. At this intersection point, one solution branch diverges downwards and $\zeta \rightarrow 0$ as $c \rightarrow \infty$; this limit is indicated by the cross at the bottom center of Fig. 10. The other branch diverges upwards and $\zeta \rightarrow 1$ ($\sigma \rightarrow -\infty$) as c increases to approach c_{crit}. This limit is indicated by the triangle at the top center in Fig. 10.

Regime 2: Characteristics of regime 2 are exhibited in mode i when $1/(2i+1)<\ell_1/L<1/(2i-1)$. The lower limit of ℓ_1/L within this regime is associated with a vertical solution branch of type 2 at $\varphi=i+1/2$, and the upper limit of ℓ_1/L is associated with a vertical solution branch of type 2 at $\varphi=i-1/2$. Curves of ζ versus φ within regime 2 are plotted in Fig. 9(b), and the characteristics of these solution branches are remarkably different from those previously observed. As before, each curve originates at $\varphi=\varphi_{oi}$ with ζ=0 (indicated by a circle); however, in this regime the curves no longer terminate with ζ=0. Rather, the damping increases monotonically and $\zeta \rightarrow 1$ ($\sigma \rightarrow -\infty$) as φ approaches the first critically damped frequency $\varphi_{crit,1}$ (22a); these limiting cases are associated with $c \rightarrow c_{crit}$ and are indicated by triangles along the top of Fig. 9(b). When $\ell_1/L=1/(2i)$, corresponding to a damper located at the first antinode of mode i, $\varphi_{crit,1}=\varphi_{oi}$, and a vertical solution branch of type 1 occurs at $\varphi=i$, as shown at the center of Fig. 9(b). Fig. 11 shows the evolution with increasing $c/\sqrt{Tm}$ of a mode shape in regime 2; the magnitude of the mode shape is plotted for ℓ_1/L=0.25 and for several different values of $c/\sqrt{Tm}$, and as $c \rightarrow c_{crit}$ and $\sigma \rightarrow -\infty$, the mode shape changes from the familiar sinusoid to a shape resembling a hyperbolic sinusoid, as indicated by (23). Interestingly, when $c>c_{crit}$, then no solution exists along a solution branch in regime 2; this indicates that if $c>c_{crit}$ vibrations are completely suppressed for modes in regime 2. However, other solutions emerge when

$c>c_{crit}$; it was previously observed that solutions with purely real eigenvalues exist only when $c>c_{crit}$, and it will be observed subsequently that solutions associated with significant vibration of the shorter cable segment also emerge when $c>c_{crit}$.

When $\ell_1/L=1/(2i-1)$, corresponding to the upper limit of regime 2, an intersection of adjacent solution branches occurs, similar to that depicted in Fig. 10. In this case, the $(i-1)^{th}$ clamped frequency and the first critically damped frequency $\varphi_{crit,1}$ are both equal to $i-1/2$, and a vertical solution branch of type 2 occurs at $\varphi= i-1/2$.

Regime 3: Characteristics of regime 3 are exhibited in mode i when $1/(2i-1)<\ell_1/L<1/i$; the lower limit of ℓ_1/L is associated with a vertical solution branch of type 2 at $\varphi=i-1/2$, and the upper limit of ℓ_1/L corresponds to a damper located at the first node of mode i. Solution branches in this regime are shown in Fig. 9(*c*) for mode 2. Each solution branch originates at φ_{oi} with $\zeta=0$, terminates at the frequency of clamped mode $i-1$ with $\zeta=0$, and attains a maximum value of ζ at an intermediate frequency. As the damper approaches the location of the first node, the frequency of clamped mode $i-1$ approaches φ_{oi}, and the solution branch for the i^{th} mode shrinks to a single point at $\varphi=i$ with $\zeta=0$. This indicates, as expected, that no damping can be added to a given mode when the damper is located at a node of that mode. Interestingly, when the damper is located at the node of mode i, a vertical solution branch of type 3 occurs at $\varphi=i$. Vertical solution branches of type 3 and 4 are associated with emergent vibrations of the shorter cable segment, and the characteristics of these solution branches are considered in the following section.

Modes with Significant Vibration in the Shorter Cable Segment

Fig. 12 depicts several solution branches associated with the first clamped mode of the shorter cable segment for several different values of ℓ_1/L, ranging from 1/3 to 1/2. Each curve originates at the clamped frequency of the shorter cable segment $\varphi_{c1}^{(1)}$ (20) with $\zeta=0$ (indicated with squares along the φ-axis in Fig. 12), and tends to the critically damped frequency $\varphi_{crit,1}^{(1)}$, (22*b*) as $\zeta\rightarrow 1$ ($\sigma\rightarrow-\infty$) (indicated with diamonds along the top of Fig. 16). Because $\varphi_{ci}^{(1)}=\varphi_{crit,i}^{(1)}$, in each case the solution branches originate and terminate at the same frequency. When $\ell_1/L=1/3$, the damper is located at the node of mode 3, and a vertical solution branch of type 3 occurs at $\varphi=3$, plotted at the right-hand edge of Fig. 12. A circle and a cross are also plotted at this frequency with $\zeta=0$ to indicate that the third undamped frequency, φ_{o3}, and the second clamped frequency, φ_{c2}, also coincide with $\varphi_{crit,1}^{(1)}$ and $\varphi_{c1}^{(1)}$ for this damper location, as can be seen

in Fig. 7. Similarly, when ℓ_1/L=1/2, the damper is located at the node of mode 2, and a vertical solution branch of type 3 occurs at φ=3. When ℓ_1/L=0.4, $\varphi_{crit,1}^{(1)}=\varphi_{c1}^{(1)}$=2.5, and a vertical solution branch of type 4 occurs at φ=2.5, plotted at the center of Fig. 12. Vertical solution branches of type 3 and 4 have similar characteristics, as discussed previously, and for each of these solution branches, the origin of the solution branch at $\zeta = 0$ is associated with $c\rightarrow\infty$, and c decreases monotonically to c_{crit} as $\zeta\rightarrow 1$ ($\sigma\rightarrow-\infty$). Consequently, if $c<c_{crit}$, then no solution exists along this type of solution branch, and these modes emerge only when $c>c_{crit}$. Fig. 13 shows a plot of the magnitude of the mode shape associated with the first clamped mode of the shorter cable segment for ℓ_1/L=0.4 and for several different values of $c/\sqrt{Tm}$. For slightly supercritical values of c, the damping is very large, and the magnitude of the mode shape resembles a hyperbolic sinusoid. As $c\rightarrow\infty$ and $\zeta\rightarrow 0$, the mode shape takes on the expected form of a half sinusoid to the left of the damper.

Global Modal Behavior

The previous discussion of the three regimes of behavior considered damper locations only up to the location of the first node, $\ell_1/\mathrm{L} \leq 1/i$. When ℓ_1/L is increased past the first node, the branches of solutions to the phase equation (10) initially exhibit the same characteristics as those observed in regime 1. As the damper is moved still further along the cable to approach the second antinode, a vertical solution branch of type 2 is encountered at a frequency of i + 1/2, and for damper locations past this point, characteristics of regime 2 are exhibited. As the damper is moved past the second antinode to approach the second node, a vertical solution branch of type 2 is encountered at a frequency of i – 1/2, and for damper locations past this point, characteristics of regime 3 are exhibited. The cycle continues past subsequent nodes and antinodes until ℓ_1/L=1/2, at which point the subsequent behavior is dictated by symmetry. This periodic cycling through the three regimes of behavior is conveyed graphically in Fig. 14. The curves of limiting frequencies versus ℓ_1/L depicted in Fig. 7 are used as the basis for this graphical depiction, and the regions corresponding to each of the three regimes have been indicated using different shadings. The shaded areas indicate ranges of φ and ℓ_1/L for which solutions to (10) exist, and the type of shading indicates the characteristics of solution branches in that region. Situations in which solution branches corresponding to two adjacent modes intersect at a vertical solution branch of type 2 (as depicted in Fig. 10) are indicated by a solid vertical line connecting the undamped frequencies of the two adjacent modes.

In the interesting case of ℓ_1/L=1/2, the damper is located at an antinode of all the odd-numbered modes and at a node of all the even-numbered modes. Vertical solution branches of type 1 then occur at the undamped frequencies of each odd-numbered mode, and $\zeta \rightarrow 1$ ($\sigma \rightarrow -\infty$) in these modes as $c \rightarrow c_{crit}$, while ζ=0 in the even-numbered modes. When $c > c_{crit}$, vibrations in the odd-numbered modes are completely suppressed, and new modes of vibration emerge, including a non-oscillatory decaying mode and a set of modes with the same frequencies as the even-numbered modes, associated with vertical solution branches of type 3. As $c \rightarrow \infty$, $\zeta \rightarrow 0$ in this set of emergent modes, and these modes take on an appearance similar to that of the undamped even-numbered mode shapes, except that they are symmetric about ℓ_1/L=1/2, with a discontinuity in slope at the damper.

CONCLUSIONS

Free vibrations of a taut cable with attached linear viscous damper have been investigated in detail, a problem that is of considerable practical interest in the context of stay-cable vibration suppression. An analytical formulation of the complex eigenvalue problem has been used to derive an equation for the eigenvalues that is independent of the damper coefficient. This "phase equation" (10) reveals the attainable modal damping ratios ζ_i and corresponding oscillation frequencies for a given damper location ℓ_1/L, affording an improved understanding of the solution characteristics and revealing the important role of damper-induced frequency shifts in characterizing the response of the system. The evolution of solution branches of (10) with varying ℓ_1/L reveals three distinct regimes of behavior. Within the first regime, when the damper-induced frequency shifts are small, an asymptotic approximate solution to (10) has been developed, relating the damping ratio ζ_i in each mode to the "clamping ratio" Θ_{ci}, a normalized measure of damper-induced frequency shift. Asymptotic approximations have also been obtained relating Θ_{ci} and ζ_i to the damper coefficient, and it is observed that these approximations grow less accurate when the damper-induced frequency shifts become large. Characteristics of the second regime are exhibited when the damper is located sufficiently near the antinode of a specific mode. For modes in this regime the damping ratio increases monotonically with the damper coefficient, approaching critical damping as the damper coefficient approaches a critical value $c_{crit} = 2\sqrt{Tm}$. When $c > c_{crit}$, vibrations are completely suppressed for modes in this regime; however, other modes of vibration emerge, including a non-oscillatory decaying mode of vibration and a set of modes with significant vibration in the shorter cable segment.

Characteristics of the solution branches in regime 3 are similar to those in regime 1 except that the oscillation frequencies are reduced, rather than increased, by the damper, and the attainable damping ratios approach zero as the damper approaches the node. A regime diagram has been presented to indicate the type of behavior that may be expected in each of the first 10 modes for any given damper location. The complexities of the solution characteristics in different regimes are potentially significant in practical applications, and the approach and analysis presented herein facilitate an improved understanding of the dynamics of the cable-damper system.

ACKNOWLEDGMENTS

The writers express sincere appreciation to the anonymous reviewers for a careful reading of the paper and for raising important questions that have allowed for a more detailed and thorough treatment of the new developments in this paper. Because of space limitations, acknowledgements to the many contributors to and sponsors of the work described in this paper are listed in the companion paper.

APPENDIX I. REFERENCES

Carne, T.G. (1981). "Guy cable design and damping for vertical axis wind turbines." *SAND80-2669,* Sandia National Laboratories, Albuquerque, NM.

Iwan, W.D., and Jones, N.P. (1984). "NATFREQ Users Manual – a Fortran IV program for computing the natural frequencies, mode shapes, and drag coefficients for taut strumming cables with attached masses and spring-mass combinations." Naval Civil Engineering Laboratory Report Number CR 94.026.

Kovacs, I. (1982) "Zur frage der seilschwingungen und der seildämpfung." *Die Bautechnik*, 10, 325-332 (in German).

Krenk, S. (2000) "Vibrations of a taut cable with an external damper." *J. Applied Mech.*, 67, 772-776.

Main, J.A. and Jones, N.P. (1999) "Full-Scale Measurements of Stay Cable Vibration." *Proc., 10th Int. Conf. on Wind Engrg.*, Balkema, Rotterdam, Netherlands, 963-970.

Main, J.A. and Jones, N.P. (2000). "A Comparison of full-scale measurements of stay cable vibration." *Proc., Structures Congress 2000*, ASCE.

Main, J.A. and Jones, N.P. (2001a). "Evaluation of viscous dampers for stay-cable vibration mitigation." *J. Bridge Engrg.,* ASCE, in press.

Main, J.A. and Jones, N.P. (2001b). "Free vibrations of a taut cable with attached damper. II: Nonlinear damper." *J. Engrg. Mech.*, ASCE, in press.

Pacheco, B.M., Fujino, Y., and Sulekh, A. (1993). "Estimation curve for modal damping in stay cables with viscous damper." *J. Struct. Engrg.*, ASCE, 119(6), 1961-1979.

Poston, R.W. (1998). "Cable-stay conundrum." *Civil Engrg.*, ASCE, 68(8), 58-61.

Rayleigh, J.W.S. (1877). *The Theory of Sound – Volume I.* Dover Publications, Inc., New York, NY, (1945 reprint).

Sergev, S.S. and Iwan, W.D. (1981). "The natural frequencies and mode shapes of cables with attached masses." *J. Energy Resources Technology*, 103(3), 237-242.

Tabatabai, H. and Mehrabi, A.B. (2000). "Design of mechanical viscous dampers for stay cables." *J. Bridge Engrg.*, ASCE, 5(2), 114-123.

Xu, Y.L., Ko, J.M., and Yu, Z. (1997). "Modal damping estimation of cable-damper systems." *Proc., 2nd Int. Symp. on Struct. and Foundations in Civ. Engrg.*, China Translation and Printing Services Ltd., Hong Kong, China, 96-102.

Yamaguchi, H. and Fujino, Y. (1998). "Stayed cable dynamics and its vibration control." *Proc. Int. Symp. on Advances in Bridge Aerodynamics.*, Balkema, Rotterdam, Netherlands, 235-253.

Yoneda, M. and Maeda, K. (1989). "A study on practical estimation method for structural damping of stay cable with damper." *Proc., Canada-Japan Workshop on Bridge Aerodynamics*, Ottawa, Canada, 119-128.

APPENDIX II. NOTATION

The following symbols are used in this paper:

A_k = coefficient of the i^{th} eigenfunction on the k^{th} cable segment;

c = viscous damper coefficient;

i = mode number;

$j = \sqrt{-1}$;

k = cable segment number;

L = length of cable;

ℓ_k = length of k^{th} cable segment;

m = mass per unit length of cable;

T = tension in cable;

t = time;

$Y_k(x_k)$ = complex mode shape on the k^{th} cable segment;

$y_k(x_k\ ,\ t)$ = transverse displacement of the k^{th} cable segment from the equilibrium position;

x_k = coordinate along cable chord axis in the k^{th} segment;

γ = displacement amplitude at the damper;

$\Delta\varphi_i$ = nondimensional difference between the i^{th} "clamped" frequency and the i^{th} undamped frequency;

ζ_i = damping ratio of mode i;

Θ_{ci} = "clamping ratio" in mode i;

λ_i = nondimensional complex eigenvalue of mode i;

σ_i = real part of the i^{th} nondimensional eigenvalue;

τ = nondimensional time;

φ_i = imaginary part of the i^{th} nondimensional eigenvalue;

φ_{ci} = i^{th} nondimensional "clamped" frequency;

$\varphi_{ci}^{(1)}$ = i^{th} nondimensional "clamped" frequency of the shorter cable segment;

$\varphi_{crit,i}$ = i^{th} nondimensional critically damped frequency;

$\varphi_{crit,i}^{(1)}$ = i^{th} nondimensional critically damped frequency of the shorter cable segment;

φ_{oi} = nondimensional undamped frequency of mode i;

ω_i = pseudoundamped natural circular frequency of mode *i*; and

ω_{o1} = undamped natural circular frequency of mode 1.

FIGURES

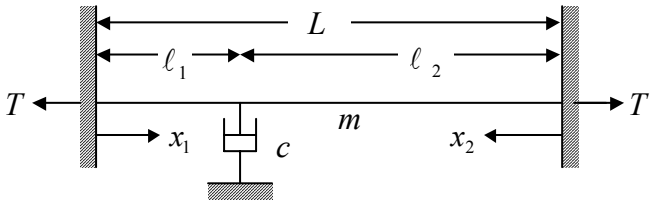

FIG. 1. Taut Cable with Viscous Damper

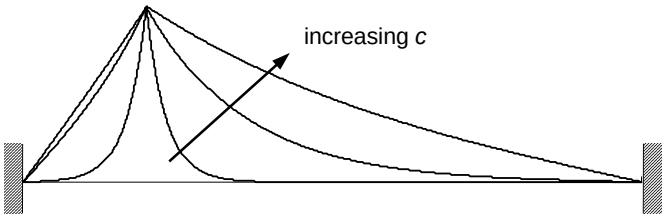

FIG. 2. Mode Shape Associated with a Purely Real Eigenvalue

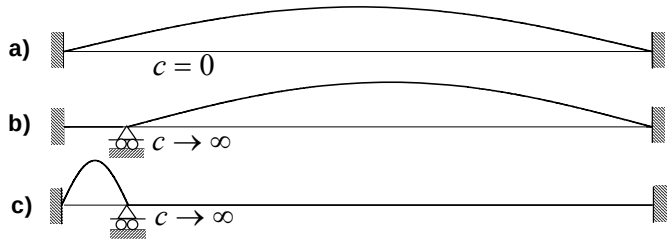

FIG. 3. Special Cases of Non-Decaying Oscillation

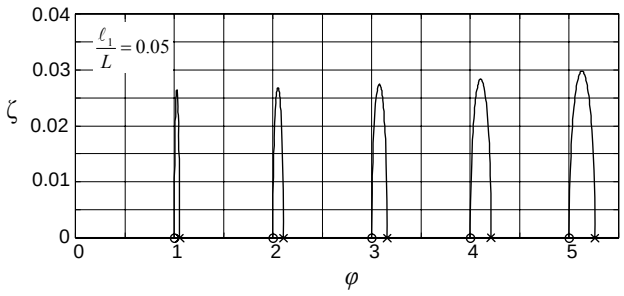

FIG. 4. Phase Equation Solution Branches (ℓ_1/L = 0.05, First 5 Modes)

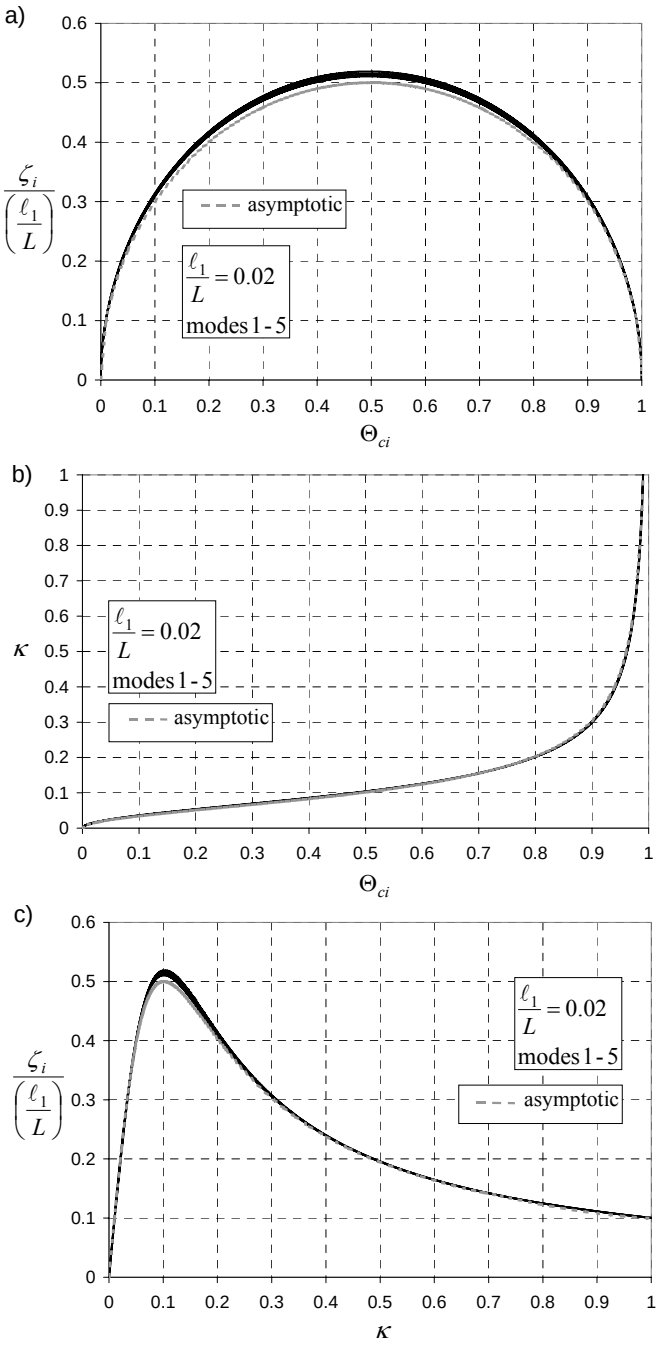

FIG. 5. (a) Normalized Damping Ratio versus Clamping Ratio; (b) Normalized Damper Coefficient versus Clamping Ratio; and (c) Normalized Damping Ratio versus Normalized Damper Coefficient.

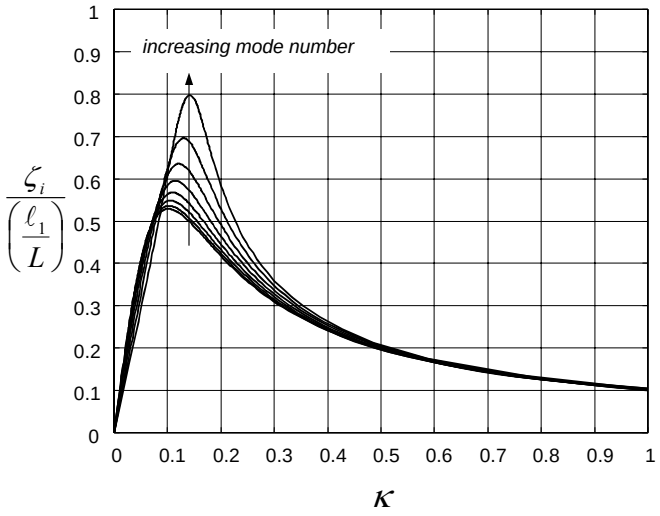

FIG. 6. Normalized Damping Ratio versus Normalized Damper Coefficient; (ℓ_1/L = 0.05, First 8 Modes)

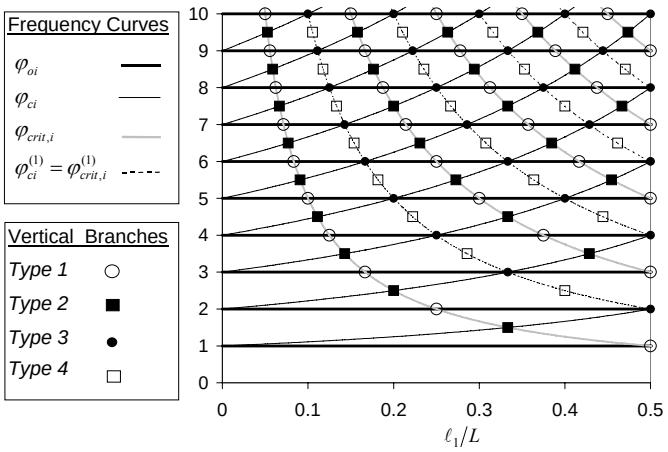

FIG. 7. Undamped Frequencies, Clamped Frequencies, and Critically Damped Frequencies versus Damper Location with Vertical Solution Branches Indicated

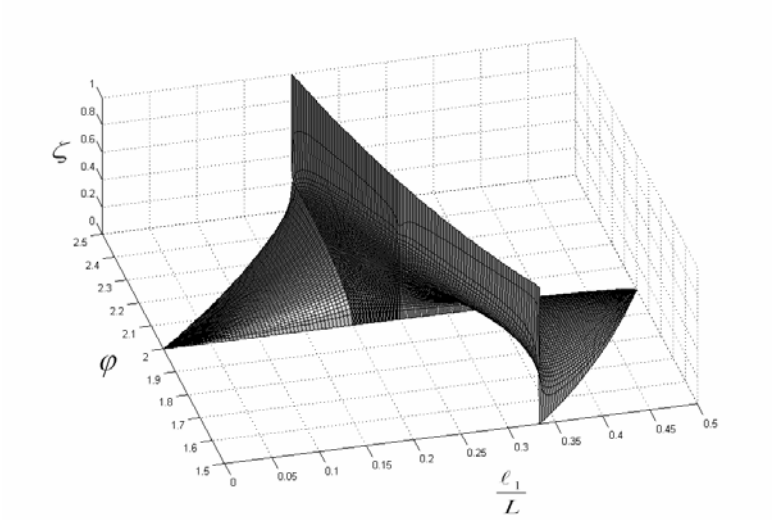

FIG. 8. Attainable Damping Ratios in Mode 2 versus Frequency and Damper Location

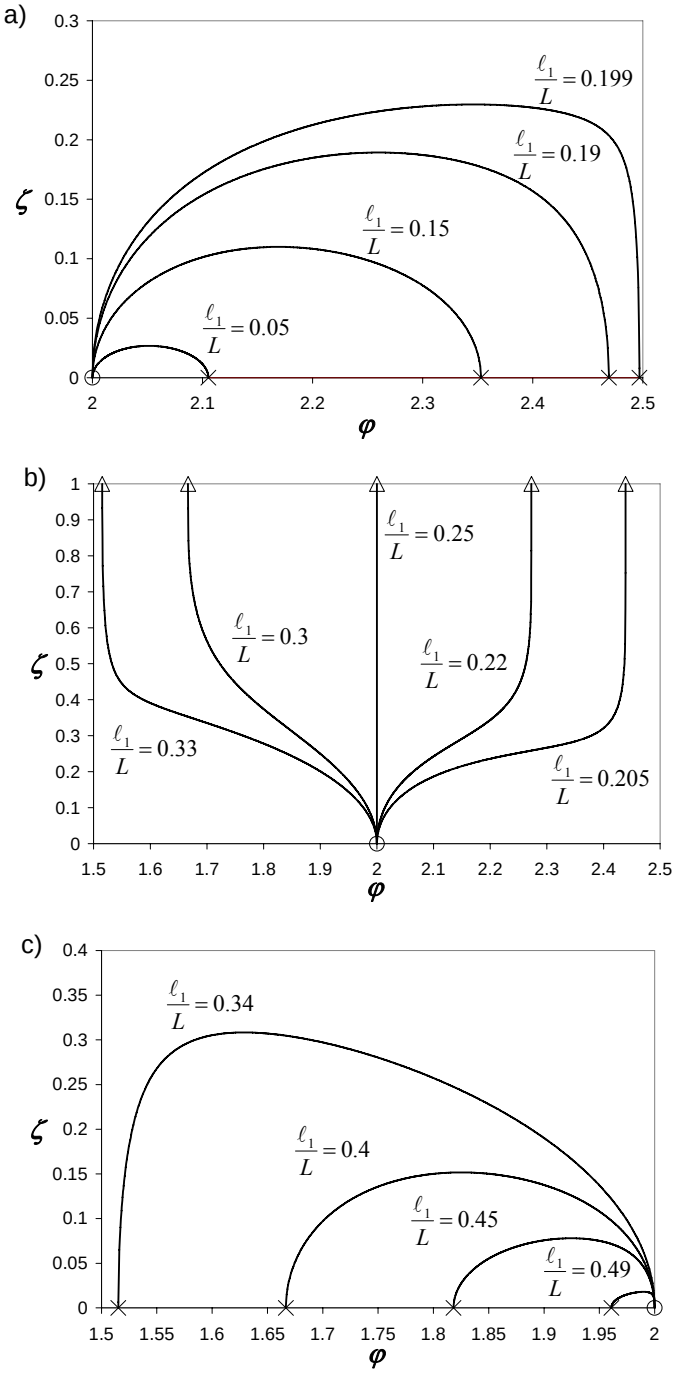

FIG. 9. Phase Equation Solution Branches for Mode 2 in Three Regimes: (a) Regime 1; (b) Regime 2; (c) Regime 3

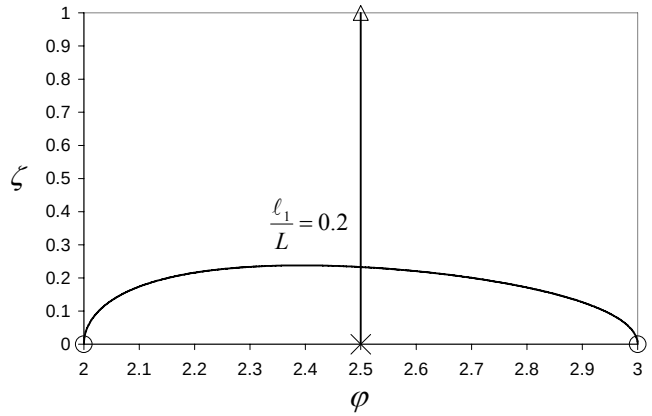

FIG. 10. Phase Equation Solution Branches for an "Intermediate Case"

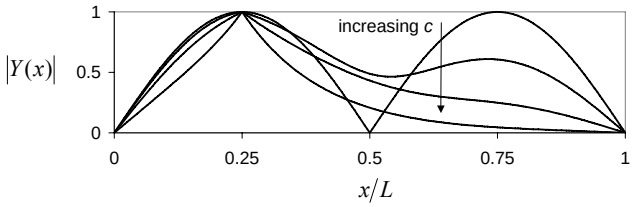

FIG. 11. Evolution with Damper Coefficient of a Mode Shape in Regime 2 (ℓ_1/L = 0.25, mode 2)

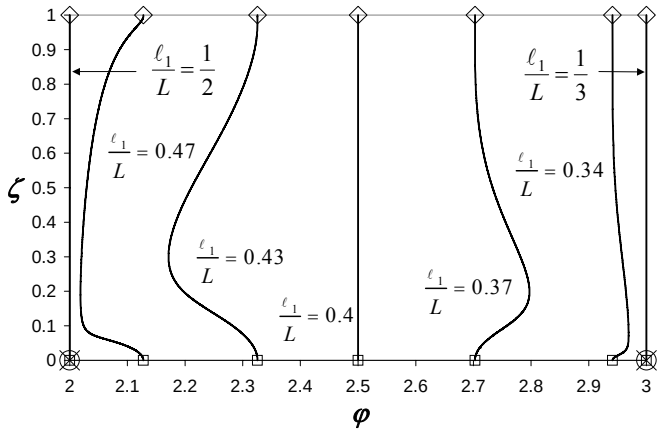

FIG. 12. Phase Equation Solution Branches Associated with the First Clamped Mode of the Shorter Segment

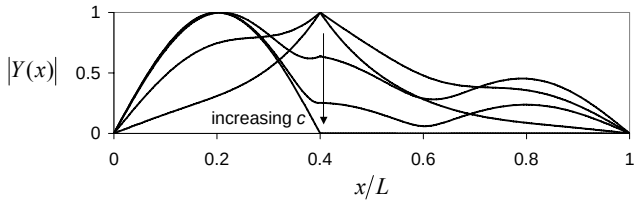

FIG. 13. Magnitude of the Eigenfunction Associated with the First Clamped Mode of the Shorter Cable Segment

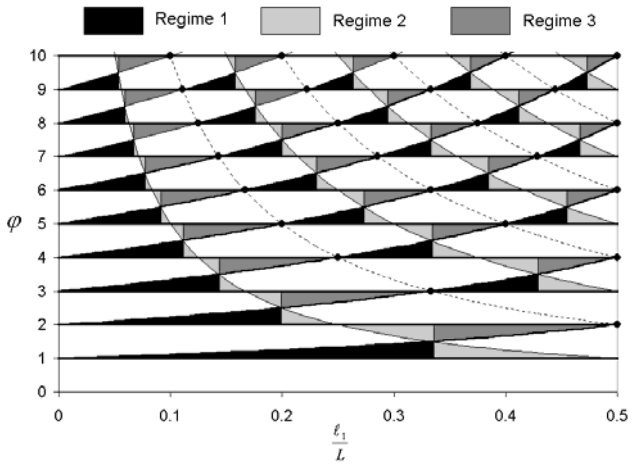

FIG. 14. Regime Diagram of Frequency versus Damper Location